

X-ray burst – accretion disk interaction in low mass X-ray binaries through the kHz quasi periodic oscillations angle

P. Peille¹, J-F. Olive¹, and D. Barret¹

¹Université de Toulouse; UPS-OMP; IRAP; Toulouse, France

and CNRS; Institut de Recherche en Astrophysique et Planétologie; 9 Av. colonel Roche, BP 44346, F-31028 Toulouse cedex 4, France

Submitted March 10, 2014

ABSTRACT

The intense radiation flux of type I X-ray bursts is expected to interact with the accretion flow around neutron stars. High frequency quasi-periodic oscillations (kHz QPOs), whose frequencies match orbital frequencies at tens of gravitational radii, offer a unique probe of the innermost disk regions. In this paper, we follow the lower kHz QPOs, in response to type I X-ray bursts, in two prototypical QPO sources, namely 4U 1636-536 and 4U 1608-522 as observed by the *Proportional Counter Array* of the *Rossi X-ray Timing Explorer*. We have selected a sample of 15 bursts for which the kHz QPO frequency can be tracked on timescales commensurable with the burst durations (tens of seconds). In a subset (3), we find evidence that the QPOs are affected by the bursts, being undetected for over ~ 80 seconds (and up to more than ~ 200 seconds in one case), while the burst emission has already decayed to a level that would enable the "pre-burst" QPO to be detected. On the other hand, for the majority of our burst-kHz QPO sample, we show that the QPO is detected as soon as the statistics allow and in the best cases, we are able to set an upper limit of ~ 20 seconds on the recovery time of the QPO. This diversity of behavior cannot be related to differences in the burst properties (rise and decay times, energetics), otherwise comparable. We discuss these results in the framework of recent findings that accretion onto the neutron star is enhanced during type I X-ray bursts. The subsequent disk depletion could explain the disappearance of the QPO for ~ 100 seconds as we observe in a subset of events. However, alternative scenarios would have to be invoked for explaining the short recovery timescales inferred from most bursts. Heating of the innermost disk regions would be a possibility, although we cannot exclude that the burst does not affect the QPO emission at all. Clearly the combination of fast timing and spectral information of type I X-ray bursts holds great potential to study the dynamics of the inner accretion flow around neutron stars. However, as we show, breakthrough observations will require a timing instrument providing at least ten times the effective area of the *RXTE/PCA*.

Key words. accretion, accretion disks – stars: individual: 4U 1636–536, 4U 1608–522 – X-rays: binaries – X-rays: bursts

1. Introduction

Illumination of accreting disks during type I X-ray bursts gives us the opportunity to study the innermost regions of the accretion flow around neutron stars (Galloway et al. 2008; Strohmayer & Bildsten 2003; Cumming 2004). Evidence for an interaction between the burst emission and the inner disk has been reported in a few individual bursts (Yu et al. 1999; Kuulkers et al. 2003; Chen et al. 2011; in't Zand et al. 2011; Serino et al. 2012; Degenaar et al. 2013). Disk depletion through radiation drag, heating of the inner disk, and even radiatively or thermally powered winds were discussed by Ballantyne & Strohmayer (2004) and Ballantyne & Everett (2005), attempting to explain the time evolution of the properties of the *superburst* of 4U 1820-303. More recently, Worpel et al. (2013), fitting the spectra of all photospheric radius expansion (PRE) bursts, as the sum of a blackbody and a scalable continuum having the shape of the pre-burst persistent emission, reported a systematic increase of the persistent emission during the burst. They interpreted this result as evidence of an accretion rate enhancement due to a rapid increase of the radiation torque on a thin accretion disk, as formalized early on by Walker (1992). A similar finding was reported by in't Zand et al. (2013) for a burst observed simultaneously by *Chandra*

and *RXTE*, although disk reprocessing of the burst emission was preferred as an alternative explanation.

In this paper, we follow a different path, by looking at kHz QPOs in response to type I X-ray bursts (see van der Klis 2006, for a review of kHz QPOs). Although there is not yet a consensus on the origin of kHz QPOs, it is generally agreed that they arise from the vicinity of the neutron star (e.g. Barret 2013), most likely in a region to be exposed to the burst emission. It is therefore worth investigating how the QPO properties react to X-ray bursts. For this purpose, we use the *RXTE* archival data of 4U 1636-536 and 4U 1608-522, known as frequent bursters (Galloway et al. 2008) and whose lower kHz QPOs can be detected and followed on burst duration timescales of tens of seconds (Barret et al. 2005, 2006).

2. Data analysis

We retrieved the archived data of the *Proportional Counter Array* (PCA) onboard *RXTE* for all the observations containing an X-ray burst for both 4U 1636-536 and 4U 1608-522, using the catalog provided by Galloway et al. (2008). In total, we obtained 172 bursts for 4U 1636-536 and 31 for 4U 1608-522 respectively. Using the *Science Events* of the PCA, we computed $1/2^{12}$ s resolution light curves from -200 to +400 s with respect to the burst peak (whenever possible, i.e. when no observation gap re-

Send offprint requests to: P. Peille, e-mail: ppeille@irap.omp.eu

Table 1. Principal characteristics of the selected X-ray bursts.

Source	Burst ID	Obs ID	Start time (<i>RXTE</i> time)	L_{peak}^a (10^{38} ergs/s)	E_{tot}^a (10^{39} ergs)	τ^a (s)	C_{pers} (cts/s)	C_{peak} (cts/s)
4U 1636-536	4	10088-01-08-030	94671416	2.68	5.54	20.7	788	9931
	6	30053-02-02-02	146144682	2.89	1.78	6.2	679	9740
	9	40028-01-02-00	162722852	2.94	1.84	6.3	569	9927
	21	40028-01-18-000	208401523	2.79	2.35	7.0	737	9916
	22	40028-01-18-00	208429016	2.76	1.85	6.7	574	10000
	23	40028-01-19-00	208740744	2.79	2.13	7.6	541	10116
	39	60032-01-09-00	242286131	1.46	1.33	9.1	417	7089
	40	60032-01-09-01	242295310	1.06	1.14	10.9	425	5355
	41	60032-01-10-00	242708641	2.00	1.50	7.5	428	9611
4U 1608-522	168	91024-01-30-10	374626248	2.98	2.06	6.9	473	9604
	4	30062-02-01-000	133389809	1.43	1.35	9.1	643	9004
	5	30062-01-01-00	133625123	2.34	2.32	9.9	543	10339
	21	70059-01-20-00	273983179	2.33	1.93	8.3	617	10562
	23	70059-03-01-000	274421898	2.39	3.16	13.2	517	10549
	24	70059-03-01-000	274434678	1.08	1.1	10.2	510	9528

Notes. ^(a) Values taken from Galloway et al. (2008). Distances of 6 and 3.6 kpc were taken to compute the peak luminosity L_{peak} and total fluence E_{tot} for 4U 1636-536 and 4U 1608-522 respectively (Pandel et al. 2008; Nakamura et al. 1989).

stricted this time interval). The date $t = 0$ was fixed for each burst at the peak count rate using 1 s resolution light curves. In order to limit the influence of the non-modulated burst photons in our analysis, while keeping enough statistics for the QPO detection, we chose to restrict our study to the 6 – 50 keV band. Indeed, the burst emission dominates in the soft X-ray band while the QPO modulated photons have a harder spectrum (Berger et al. 1996).

2.1. Data reduction

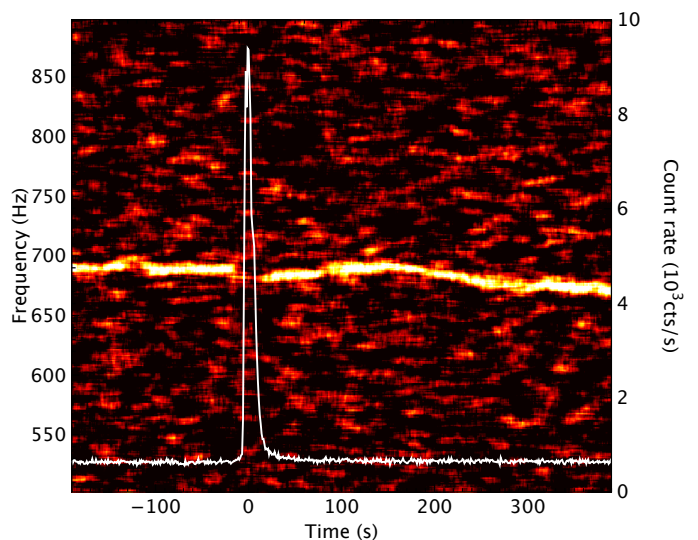
Dynamical Fourier Power Density Spectra (PDS) containing the time series of Leahy normalized PDS (Leahy et al. 1983) were computed. These spectra were obtained with an integration time of 1 s and a Nyquist frequency of $f_{\text{Ny}} = 2048$ Hz. Segments of data containing an X-ray burst and a QPO detectable on short timescales (~ 20 – 30 s) were identified. A list of 10 and 5 bursts in 4U 1636-536 and 4U 1608-522 respectively was so obtained (see Table 1 for a summary of the main properties of these bursts).

2.2. Initial results

The most common pattern observed in the dynamical PDS is illustrated in Fig. 1: the QPO is clearly detected both before and after the X-ray burst at about the same frequency (i.e. no significant frequency jumps are observed), but in an interval of ~ 20 – 30 s after the onset, the QPO is not detected. This non detection can be explained by the addition of the non-modulated burst photons¹. This pattern is however not observed in three bursts of 4U 1636-536, for which the QPO remains undetected for up to several hundreds of seconds, while the overall source emission has returned to the level it had before the burst (see Fig. 2).

We now wish to simulate the effect of the burst photons on the QPO detectability. For this purpose, we have first estimated the QPO parameters (amplitude, frequency, width), using segments of 100 seconds prior to the bursts (corresponding to 20

¹ The significance of an excess power is proportional to $\frac{S^2}{S+B} \text{rms}^2$ where S and B correspond to the signal and background count rates respectively, and rms to the fractional amplitude of the QPO emission (van der Klis 1989). A burst corresponds to a large increase of B , leading the signal to disappear in the dynamical PDS.

**Fig. 1.** Dynamical PDS and light curve (white line) around burst n°4 of 4U 1608-52. The image corresponds to a series of 1 s PDS plotted as a function of time, convolved with a 6 Hz and 20 s averaging kernel for better visibility. Power is color coded with a linear scale between 2 (black) and 3 (white).

PDS of 5 seconds duration, stepped by 10 seconds). The QPO whose detection is highly significant for this integration time was fitted by a Lorentzian with the maximum likelihood method described in Barret & Vaughan (2012). A persistent emission light curve with the same time resolution as the data ($1/2^{12}$ s) containing such a QPO was then randomly simulated following Timmer & Koenig (1995). The burst light curve was itself computed on the same time resolution, starting from the interpolation of the one recorded with one second time bins. Poisson noise fluctuations were added to high-time resolution burst light curve, which was then added to the light curve of the persistent emission containing the QPO. The summed light curve was then processed the same way as the real data to produce 1 second PDS. This procedure was repeated 10 000 times. PDS were averaged within the non detection gap for both the data and the simulations, and

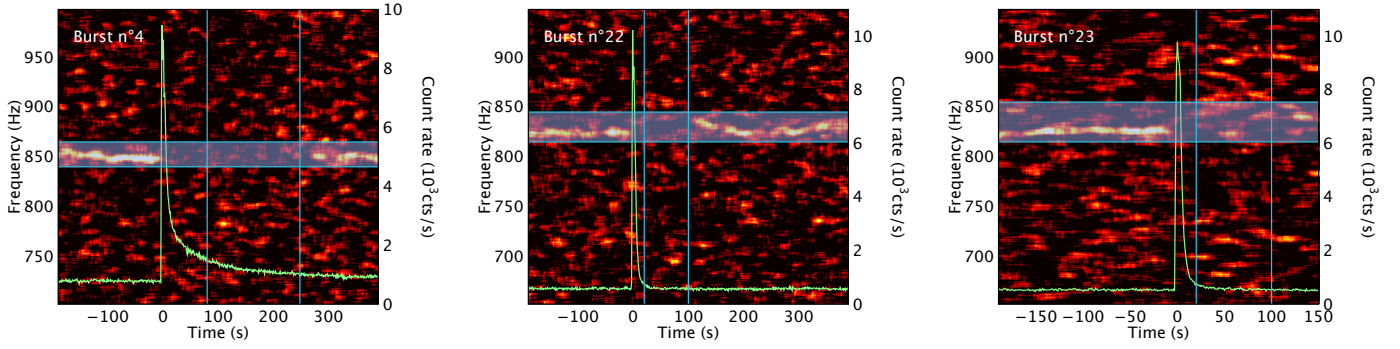


Fig. 2. Dynamical PDS and light curves (green lines) around bursts n°4 (left), 22 (middle) and 23 (right) of 4U 1636-536. The image corresponds to a series of 1 s PDS plotted as a function of time, convolved with a 6 Hz and 20 s averaging kernel for better visibility. Power is color coded with a linear scale between 2 (black) and 3 (white). The blue zones and vertical lines represent the time and frequency intervals used to probe the significance of the QPO non detection in the simulations, namely [80;250 s] and [840;865 Hz] for burst n°4, [20;100 s] and [815;845 Hz] for n°22, and [20;100 s] and [815;855 Hz] for n°23. Note that for burst n°23 an observation interruption limits the analysis to ~ 150 s after the burst.

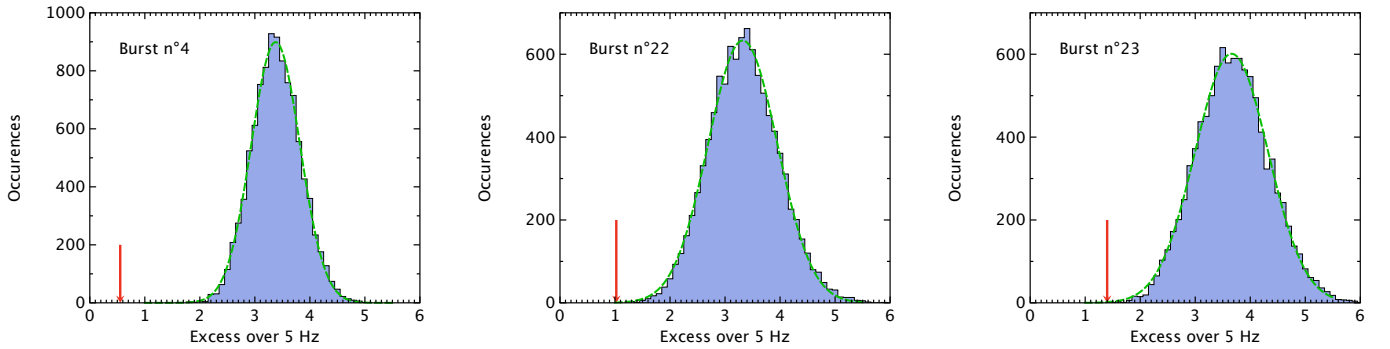


Fig. 3. Results of the PDS simulations for bursts n°4 (left), 22 (middle) and 23 (right) of 4U 1636-536. The blue histograms correspond to the distribution of the excesses found in the simulations (see text), the red arrows to the values found in the data and the green dashed lines to gaussian fits of the distributions.

excesses of power were searched over the same frequency interval around the QPO frequency in a 5 Hz window (see Fig. 2). In conditions representative of the three bursts, the simulations systematically reproduced an excess of power larger than the one found in the data, strongly suggesting that the QPO was affected by the burst (see Fig. 3). Another way of inferring this conclusion is by comparing the RMS amplitude of the QPO prior to the burst and the RMS upper limit on the QPO during the non detection gap, considering the QPO width unchanged and the burst photons contributing to the noise. As listed in Table 2, 90% confidence level upper limits are significantly below the QPO RMS measured prior to the burst. On the other hand, for all the other bursts of 4U 1636-536 (and 4U 1608-522), the RMS amplitude of the QPO measured before and after the burst are consistent with one another, as shown in Fig. 4 (see Table 2 for more detail). Note that in order to take into account the changing count rate during the burst decay and the fact that burst photons are not modulated, the rms amplitude of the QPO has been computed from the Lorentzian normalization factor R (Barret & Vaughan 2012) using the following relation:

$$\text{rms} = \sqrt{\frac{T}{C_{\text{pers}}^2 \sum_t 1/C(t)}} R \quad (1)$$

where $C(t)$ is the one second resolution count rate in the time interval of duration T and C_{pers} the one in the persistent emission.

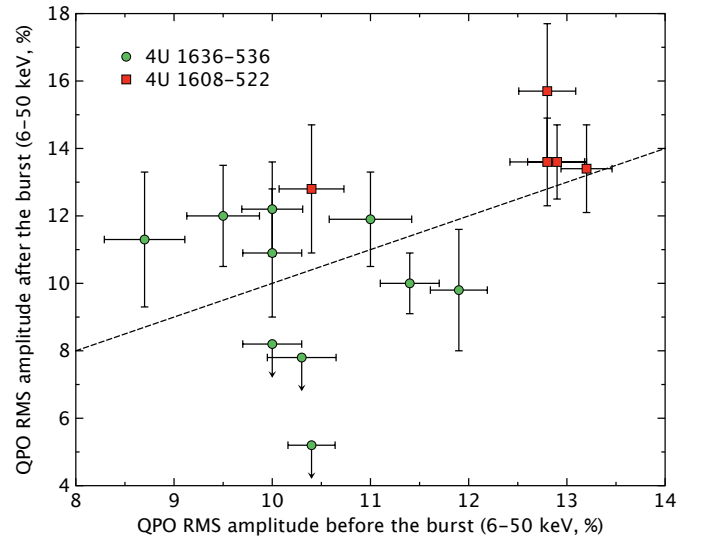


Fig. 4. Distribution of the QPO rms amplitude measured after the burst against the one measured before the burst (see Table 2). The green circles correspond to bursts of 4U 1636-536, the red squares to bursts of 4U 1608-522. The dashed line corresponds to equal amplitudes before and after the burst.

2.3. Stacking of the bursts

As shown in Figure 4, our sample of QPOs from 4U 1608-522 is rather homogenous. In addition, for 4U 1608-522, the QPOs are

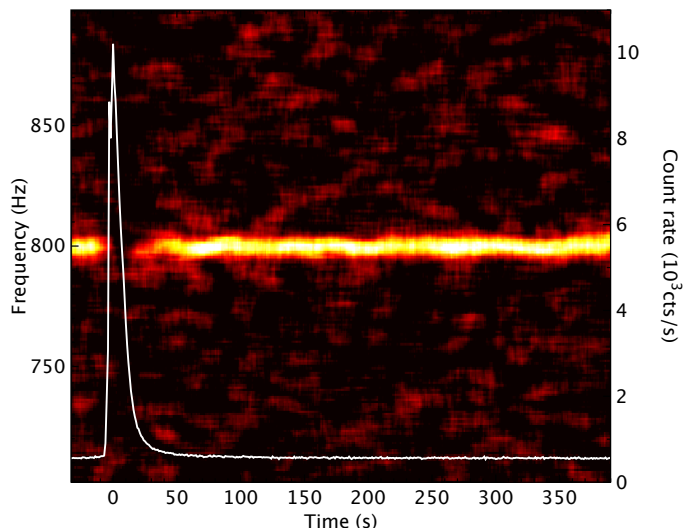


Fig. 5. Dynamical PDS and mean light curve (white line) resulting from the stacking of all the 4U 1608-52 observations. The image corresponds to the succession of 1 s PDS plotted as a function of time, convolved with a 6 Hz and 20 s averaging kernel for better visibility. Power is color coded with a linear scale between 2 (black) and 3 (white). Note that the plot starts at -43 s because of an observation gap for burst n°21.

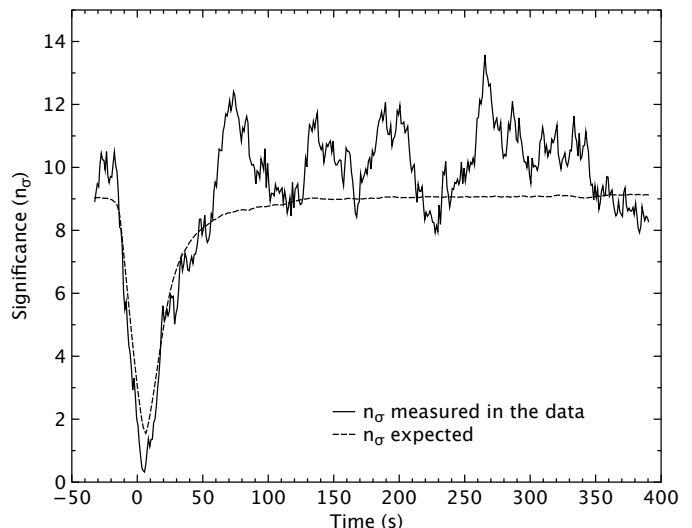


Fig. 6. Significance of the maximum excess over 4 Hz in the [790;810 Hz] band as a function of time in the dynamical PDS resulting from the stack of the 4U 1608-52 observations (see text). The solid line corresponds to significance values measured in the data while the dashed line is the level expected from the burst light curves and QPO profiles measured before the burst. Note that the plot starts at -43 s because of an observation gap for burst n°21.

easier to track on short timescales than for 4U 1636-536. As a way to improve our QPO detection sensitivity around the burst, one can combine the PDS from different bursts, after aligning them to a reference frequency. The QPO frequency was tracked before and after the burst using an algorithm similar to the one presented in Barret et al. (2006), which uses the centroid of the excess power as a proxy of the QPO frequency (when the significance of the QPO is not sufficient to obtain a stable fit). We have checked through extensive Monte Carlo PDS simulations of QPOs of varying frequency, in the presence of a typical X-ray burst of 4U 1608-522, that such an algorithm did not introduce any systematic biases in the recovered QPO parameters, and is therefore suitable for combining PDS of different bursts. The dynamical PDS produced for 4U 1608-522 is shown in Fig. 5, after having aligned all the PDS to a 800 Hz reference frequency. Clearly the non detection gap is now restricted to very close to the burst peak. For indication, a 6.6σ excess of power is detected in a 15 seconds long interval, 15 seconds after the burst peak. We have thus set a conservative upper limit of ~ 20 seconds on the QPO reappearance or on its recovery time.

Sliding a 20 seconds window over the burst (with 1 second step), one can track the evolution of the significance of the QPO detection as a function of time, and compare it to the one for which the QPO parameters are unchanged during the bursts and only the burst photons add to the noise to lower the detection significance. This is shown in Fig. 6: the solid curve shows the evolution of the significance of the maximum power excess over 4 Hz (total power exceeding the Poisson level of 2) measured as a function of time in the stacked PDS between 790 and 810 Hz. The dashed one corresponds to the level expected assuming that the QPO parameters measured before the burst do not change during the burst. It is remarkable how close the observed and predicted profiles are comparable², suggesting that for our sam-

ple of 4U 1608-522 bursts, the QPOs were unaffected by the presence of the bursts.

3. Comparison with burst parameters

In the above analysis, we have shown that not all QPOs respond the same way to type I X-ray bursts. Here we wish to investigate whether this can be related to changes in the burst parameters. In Fig. 7, we plot the ratio of the RMS amplitude of the QPO after and before the burst, against the peak luminosity and burst fluence. As can be seen, no clear trend is observed within the limited sample of the bursts considered in our analysis, although for the three bursts for which the QPO disappeared long after the burst in 4U 1636-536, their peak luminosity lies on the high part of the diagram, and one of them (the longest one, see Fig. 2, left panel) has an exceptionally large fluence.

We have also performed a spectral analysis of our burst sample following the recent work of Worpel et al. (2013), where the time resolved burst spectrum is fitted as the sum of an absorbed blackbody and a scalable persistent emission spectrum (with a scaling factor f_a), as fitted before the burst. Fixed hydrogen column densities of $N_H = 0.36 \times 10^{21}$ (Pandel et al. 2008) and $1.1 \times 10^{21} \text{ cm}^{-2}$ (Güver et al. 2010) were used for 4U 1636-536 and 4U 1608-522 respectively. Spectra were fitted in the 2.5 keV – 20 keV band using xpspec version 12.8. Burst spectra were extracted with variable time steps matching the burst dynamics. Two different models were used to fit the persistent emission spectrum: `wabs*(nthcomp+diskline)` for 4U 1636-536 and `wabs*(nthcomp+gaussian+bbbodyrad)` for 4U 1608-522. As discussed by Worpel et al. (2013), what matters is to have a model describing accurately the persistent emission before the bursts. Those models both provide good and stable fits. Like Worpel et al. (2013), we found that f_a increases during the peak phase (up to 20 or so, with typical values around 5), and remains significantly above 1 over the 20 seconds interval following the burst. An example of f_a variations for three bursts is

² The small difference between the two curves in the persistent emission after the burst is due to the fact that the measurement of the power excess used here is sensible to positive noise fluctuations above the QPO profile.

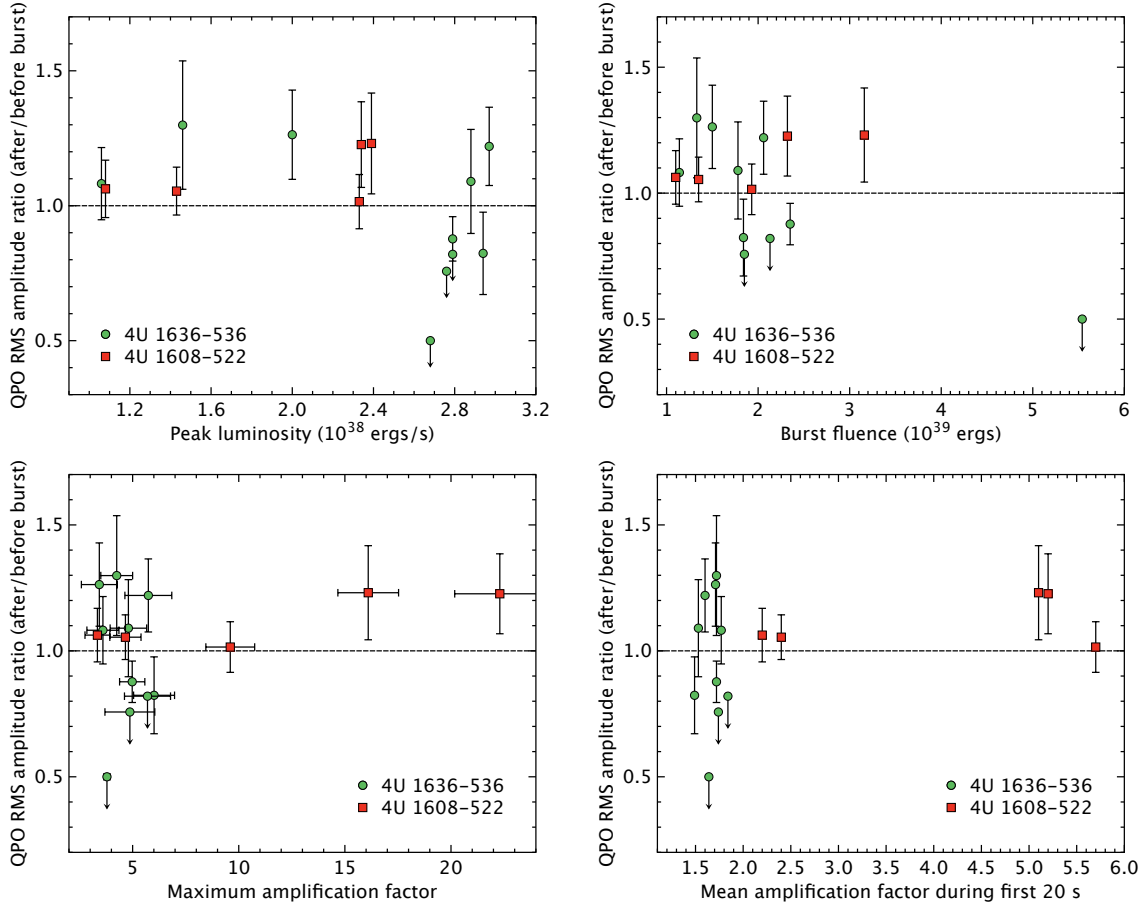


Fig. 7. Ratio of the kHz QPO rms level after the burst over its value before the burst as a function of the burst peak luminosity (upper left), burst fluence (upper right), maximum f_a (lower left) and mean f_a during the first 20 seconds (lower right). The green circles correspond to bursts of 4U 1636-536, the red squares to bursts of 4U 1608-522. When no significant signal was detected, upper limits were plotted (bursts n°4, 22 and 23 of 4U 1636-536).

shown in Fig. 8. No correlation was found between the ratio of the QPO RMS amplitude before and after the burst and f_a , either its maximum value or its mean value over the first 20 seconds interval (as shown in Fig. 7). Yet, it is interesting to note that with the exception of the long burst of 4U 1636-536 (Fig. 2, left panel), f_a has returned to 1 within 20 seconds. This latter value is commensurable with the recovery time inferred from the staking of the 4U 1608-522 data.

4. Discussion

High frequency QPOs are commonly believed to be generated close to the neutron star surface or in the innermost parts of the accretion disk. Similarly, type I X-ray bursts are produced on the neutron star surface and radiate away enough energy to change the proprieties of the accretion flow. It is therefore natural to investigate the impact of a type X-ray burst on kHz QPOs. Our finding that there may be cases where the QPO is affected by the bursts on hundreds of second timescales, and cases where the QPO does not suffer from the bursts down to the shortest timescales that can be investigated by current data (~ 20 seconds) is clearly puzzling, especially because those two behaviors cannot be connected to different properties of the bursts, such as the burst peak luminosity. Let us now discuss our results in the framework of the recent work by Worpel et al. (2013), claiming that the accretion rate is enhanced during type I X-ray bursts.

4.1. A disk recession ?

As accretion disks are optically thick in the radial direction, an enhanced accretion rate due to radiation torque can only be attained through disk depletion: $f_a > 1$ implies a receding disk. The Eddington-scaled accretion rate in our data sets is ~ 0.12 and $0.04 \dot{M}_{\text{Edd}}$ for 4U 1636-536 and 4U 1608-522 respectively, using a neutron star mass of $1.4 M_{\odot}$. If we take conservative values for the mean f_a measured during the 20 s following the burst onset of 1.5 and 2 for the two sources, this gives depleted masses of at least $\sim 3 \times 10^{18}$ and 2×10^{18} g. Using standard accretion disks as described in Shakura & Sunyaev (1973) to model the mass repartition in the inner parts of the disk with an α -parameter of 0.1, these masses correspond approximately to the mass contained between $7-50 R_g$ for 4U 1636-536, and $7-30 R_g$ for 4U 1608-522. It is important to note that the disk surface density scales as $1/\alpha$ which is poorly constrained and that these masses are only rough estimates.

An estimate of the time scale at which the disk recovers its former geometry is given by the viscous time (Frank et al. 2002, Eq. 5.69):

$$t_{\text{visc}} \sim 3 \times 10^5 \alpha^{-4/5} \left(\frac{\dot{M}}{10^{16} \text{ g/s}} \right)^{-3/10} \left(\frac{M}{M_{\odot}} \right)^{1/4} \left(\frac{R}{10^{10} \text{ cm}} \right)^{5/4} \text{ s} \quad (2)$$

with R the distance to the neutron star center, \dot{M} the accretion rate and M the neutron star mass. For $M = 1.4 M_{\odot}$, $\alpha = 0.1$ and

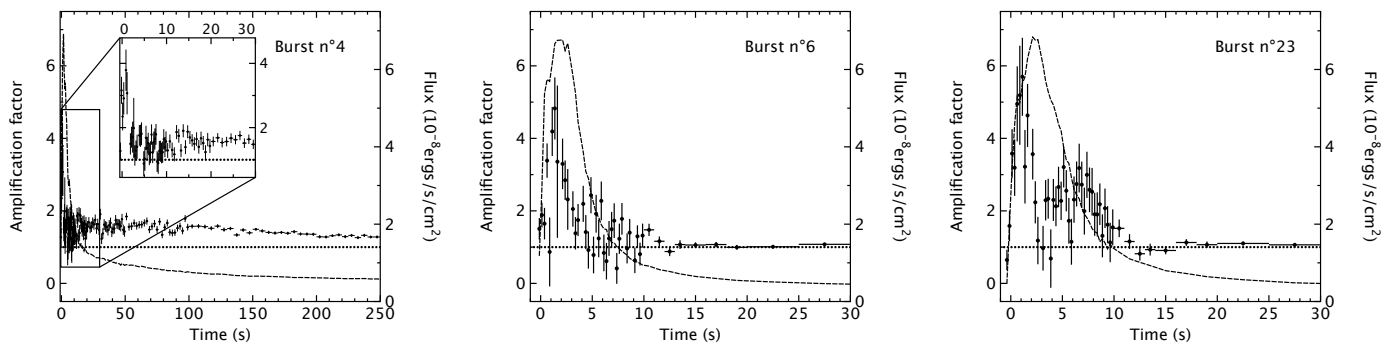


Fig. 8. Amplification factor (f_a) profiles (points with error bars) obtained from the spectral analysis of bursts n°4 (left), 6 (middle) and 23 (right) of 4U 1636-536. For the longer burst n°4, the first 30 seconds of the f_a profile have been magnified for better comparison. The dashed lines correspond to the burst light curves, and the dotted horizontal lines to $f_a = 1$.

with the appropriate accretion rates, we find $t_{\text{visc}} \sim 130$ s at $50 r_g$ from 4U 1636-536 and $t_{\text{visc}} \sim 100$ s at $30 r_g$ from 4U 1608-522. It is worth noting that increasing α gives shorter viscous times, but it also increases the radius matching the loss of mass and similar time scales are found. Within all the caveat of the above assumptions, it is interesting to note that those timescales match the non detection gap of the two shorter bursts from 4U 1636-536, shown in Fig. 2. Note however that for the longer burst of 4U 1636-536, f_a is still above 1 while the QPO reappears (see Fig. 8), arguing against the idea that the disk is still truncated through depletion. This clearly suggests some cautions when using f_a to derive the accretion rate during the burst. The found timescales are also a factor of 5-10 longer than the recovery time we inferred from 4U 1608-522, thus suggesting that an alternative to disk depletion should be considered.

4.2. Heating of the inner region ?

To reduce the viscous disk recovery time, only the innermost part of the accretion disk should be affected. At $10 R_g$, the viscous time ~ 18 s for 4U 1636-536 and ~ 25 s for 4U 1608-522 with an α -parameter of 0.1. One possibility could thus be disk irradiation by the burst photons, that is expected to produce significant heating, and leading potentially the disk to puff up (Ballantyne & Everett 2005). Such a mechanism may thus be consistent with the short recovery times of the QPOs from 4U 1608-522. Unfortunately, current data cannot tell us what happens to the QPO within the first 20 seconds, e.g. whether its amplitude drops or its coherence decreases. Hence, although that seems unlikely, we cannot either exclude that there is no effect of the burst on the QPO.

Existing data are therefore insufficient to access timescales shorter than 20 seconds, while we would like to measure the QPO parameters as close as possible to the burst peak. Assuming that the QPO amplitude and width remain constant within the burst and only the QPO frequency varies, in Fig. 9 we show that a new generation timing instrument like the *LOFT/LAD* (Feroni et al. 2012) would enable to track the QPO frequency, even at the burst peak. Tracking the QPO frequency along the frequency drift assumed in the simulation requires an increase in effective area by at least an order of magnitude (15 in the case considered here³). This simulation illustrates how such a large area timing instrument could deliver breakthrough observations

³ *LOFT/LAD* response files were downloaded from <http://www.isdc.unige.ch/loft> for the simulation. We have assumed the goal effective area of 12 m^2 at 8 keV for the *LAD*.

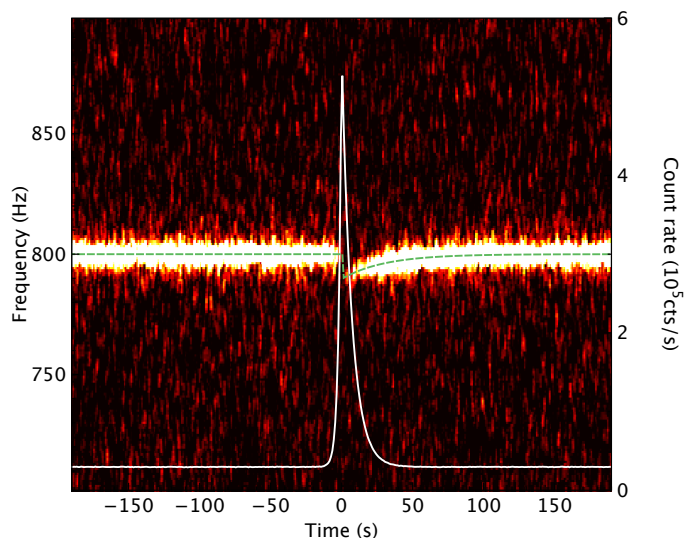


Fig. 9. Simulated dynamical PDS containing a QPO at 800 Hz and a smooth frequency jump of 10 Hz initiated at the burst peak (green dashed line). The QPO rms is 8% and the QPO width is 3 Hz. The *LOFT/LAD* 3–30 keV light curve of the type I X-ray burst (peak at 18 times the persistent emission level, rise time of 2 seconds and decay time of 7 seconds) is overplotted with a white line. The persistent count rate was estimated using 4U 1608-522 as the source. The image corresponds to a series of 1 s PDS plotted as a function of time, convolved with a 6 Hz and 2 s averaging kernel. Power is color coded. Note that the color scale is different from the one used for *RXTE* data: it saturates at a power level of 8 instead of 3.

on the burst-QPO interaction, providing at the same time insights on the location of the QPO modulated emission.

4.3. Conclusions

The interaction between the kHz QPO signals and type-I X-ray bursts has been studied in two LMXBs: 4U 1636-536 and 4U 1608-522. Two types of behaviors of different timescales have been identified. We have found clear evidence for an interaction of the burst with the QPO emission in a subset of our sample, while for most of them, within the current data, the QPO does not seem to be affected by the burst. We have set an upper limit of 20 seconds for the recovery time of the QPO in 4U 1608-522. We have shown that a next generation timing mission providing an increase in effective area of at least an order of magnitude, such as *LOFT*, would be able to detect the QPO throughout the bursts

Table 2. kHz QPO shapes before and after the X-ray bursts.

Source	Burst ID	Freq _{pers}	R _{pers}	rms _{pers} (%)	w _{pers} (Hz)	Freq _{burst}	R _{burst}	rms _{burst} (%)	w _{burst} (Hz)
4U 1636-536	4	848	8.5±0.4	10.4±0.2	3.5±0.3	(u.l.)	1.4 (u.l.)	5.2 (u.l.)	(u.l.)
	6	874	6.7±0.4	10.0±0.3	4.3±0.4	876±2.5	7.9±2.8	10.9±1.9	13.8±6.3
	9	862	8.2±0.4	11.9±0.3	5.5±0.4	855±0.6	5.3±1.9	9.8±1.8	4.8±3.0
	21	859	9.5±0.5	11.4±0.3	5.6±0.5	854±0.4	7.2±1.3	10.0±0.9	3.5±0.9
	22	823	5.9±0.4	10.3±0.3	3.9±0.3	(u.l.)	3.3 (u.l.)	7.8 (u.l.)	(u.l.)
	23	825	5.4±0.3	10.0±0.3	2.2±0.2	(u.l.)	3.4 (u.l.)	8.2 (u.l.)	(u.l.)
	39	802	3.2±0.3	8.7±0.4	2.0±0.4	796±2.1	5.1±1.8	11.3±2.0	8.3±3.8
	40	843	5.2±0.4	11.0±0.4	4.2±0.5	839±0.5	5.7±1.3	11.9±1.4	3.7±1.3
	41	820	3.9±0.3	9.5±0.4	2.7±0.3	826±0.7	5.5±1.4	12.0±1.5	5.0±1.7
	168	849	4.9±0.3	10.0±0.3	2.7±0.3	849±0.7	6.7±1.5	12.2±1.4	5.3±1.6
4U 1608-522	4	689	10.9±0.5	12.9±0.3	5.6±0.3	684±0.5	10.9±1.8	13.6±1.1	5.5±1.3
	5	740	8.8±0.4	12.8±0.3	4.7±0.3	722±1.2	11.6±3.0	15.7±2.0	12.1±4.4
	21 ^a	703	10.8±0.4	13.2±0.3	4.7±0.3	704±0.8	10.1±2.0	13.4±1.3	7.9±2.1
	23	813	5.8±0.4	10.4±0.3	4.1±0.3	801±2.8	6.0±1.8	12.8±1.9	6.7±2.8
	24	805	8.5±0.5	12.8±0.4	5.7±0.5	790±0.5	9.3±1.8	13.6±1.3	5.3±1.5

Notes. For the bursts n°4, 22 and 23 of 4U 1636-536, the QPO rms amplitude upper limits were computed during the non detection gap, namely [80;248 s] for the first one and [20;100 s] for the other two using the pre-burst width as well as a frequency fixed to the position of the most significant excess (noted u.l. in the table). For all other bursts, the QPO parameters after the burst were computed in the same time interval, 20 to 100 seconds, after the burst peak.

^(a) For this one, not enough data were recorded before the burst and the QPO parameters have been estimated away from the burst (200 seconds after), and taken as representative of the QPO parameters before the burst.

and hence provide better constraints on the physics of the interaction of the burst emission and its surroundings. This would need to be complemented by theoretical work aiming at a better modeling of the burst-disk interaction.

Acknowledgements. This research has made use of data obtained through the High Energy Astrophysics Science Archive Research Center On-line Service, provided by the NASA/Goddard Space Flight Center. We thank Duncan K. Galloway and Hauke Worpel for helpful conversations and suggestions.

References

- Ballantyne, D. R. & Everett, J. E. 2005, *ApJ*, 626, 364
 Ballantyne, D. R. & Strohmayer, T. E. 2004, *ApJ*, 602, L105
 Barret, D. 2013, *ApJ*, 770, 9
 Barret, D., Kluźniak, W., Olive, J. F., Paltani, S., & Skinner, G. K. 2005, *MNRAS*, 357, 1288
 Barret, D., Olive, J.-F., & Miller, M. C. 2006, *MNRAS*, 370, 1140
 Barret, D. & Vaughan, S. 2012, *ApJ*, 746, 131
 Berger, M., van der Klis, M., van Paradijs, J., et al. 1996, *ApJ*, 469, L13
 Chen, Y.-P., Zhang, S., Torres, D. F., et al. 2011, *A&A*, 534, A101
 Cumming, A. 2004, *Nuclear Physics B Proceedings Supplements*, 132, 435
 Degenaar, N., Miller, J. M., Wijnands, R., Altamirano, D., & Fabian, A. C. 2013, *ApJ*, 767, L37
 Feroci, M., Stella, L., van der Klis, M., et al. 2012, *Experimental Astronomy*, 34, 415
 Frank, J., King, A., & Raine, D. J. 2002, *Accretion Power in Astrophysics: Third Edition*
 Galloway, D. K., Muno, M. P., Hartman, J. M., Psaltis, D., & Chakrabarty, D. 2008, *ApJS*, 179, 360
 Güver, T., Özel, F., Cabrera-Lavers, A., & Wroblewski, P. 2010, *ApJ*, 712, 964
 in't Zand, J. J. M., Galloway, D. K., & Ballantyne, D. R. 2011, *A&A*, 525, A111
 in't Zand, J. J. M., Galloway, D. K., Marshall, H. L., et al. 2013, *A&A*, 553, A83
 Kuulkers, E., den Hartog, P. R., in't Zand, J. J. M., et al. 2003, *A&A*, 399, 663
 Leahy, D. A., Darbro, W., Elsner, R. F., et al. 1983, *ApJ*, 266, 160
 Nakamura, N., Dotani, T., Inoue, H., et al. 1989, *PASJ*, 41, 617
 Pandel, D., Kaaret, P., & Corbel, S. 2008, *ApJ*, 688, 1288
 Serino, M., Mihara, T., Matsuoka, M., et al. 2012, *PASJ*, 64, 91
 Shakura, N. I. & Sunyaev, R. A. 1973, *A&A*, 24, 337
 Strohmayer, T. & Bildsten, L. 2003, *ArXiv Astrophysics e-prints*
 Timmer, J. & Koenig, M. 1995, *A&A*, 300, 707
 van der Klis, M. 1989, in *Timing Neutron Stars*, ed. H. Ögelman & E. P. J. van den Heuvel, 27
 van der Klis, M. 2006, *Rapid X-ray Variability*, 39–112
 Walker, M. A. 1992, *ApJ*, 385, 642
 Worpel, H., Galloway, D. K., & Price, D. J. 2013, *ApJ*, 772, 94
 Yu, W., Li, T. P., Zhang, W., & Zhang, S. N. 1999, *ApJ*, 512, L35